NUMERICAL SIMULATION OF AIR FLOW OVER BREAKING WAVES

N. MAAT[1] and V. K. MAKIN

Division of Oceanographic Research, Royal Netherlands Meteorological Institute (KNMI), P.O. Box 201, 3730 AE De Bilt, The Netherlands

(Received in final form 2 December, 1991)

Abstract. The air flow above breaking monochromatic Stokes waves is studied using a numerical nonlinear model of the turbulent air flow above waves of finite amplitude. The breaking event (spilling breaker) is parameterized by increasing the local roughness at the downwind slope of the wave, just beyond the crest. Both moderate slope waves and steep waves are considered. Above steep breaking waves, a large increase (typically 100%) in the total wind stress – averaged over the wave profile – is found compared to nonbreaking moderate slope waves. This is due to the drastic increase of the form drag, which arises from the asymmetrical surface pressure pattern above breaking waves. Both increase of wave slope (sharpening of the crest) and increase of local roughness in the spilling breaker area cause this asymmetrical surface pressure pattern. A comparison of the numerical results with the recent experimental measurements of Banner (1990) is carried out and a good agreement is found for the structure of the pressure pattern above breaking waves and for the magnitude of enhanced momentum transfer.

1. Introduction

A large part of the total wind stress above the sea surface can be formed by wave-induced stress. Under high wind conditions the short waves (length less than 1 m) are strongly involved in breaking processes. The mechanism of momentum and energy transfer to breaking waves is complicated and not fully understood (see e.g., discussion in Banner (1990)). Wave breaking at sea occurs within a full spectrum of wave components, making measurements and analysis very difficult. Considerable simplification to study the breaking waves can be achieved in laboratory conditions, where a monochromatic breaking wave pattern can be generated.

A detailed experimental study of air flow above breaking monochromatic waves was recently reported by Banner (1990). The pressure distribution was measured above a "stationary breaking wave configuration" and above a train of continuously breaking mechanically triggered waves. The results showed pressure phase shifts and patterns of wave pressure distribution which are closely paralleled. Banner's results indicate that the breaking event (spilling breaker) influences the distribution of the wave-induced pressure field just above the wave surface. He reports a large increase (typically 100%) of the total wind stress above breaking waves, this increase being due to the increase of wave-coherent momentum flux (form drag) associated with actively breaking waves. The form drag is formed by the correlation of the pressure field with the wave slope. A highly asymmetrical

[1] *Also:* Dept. of Applied Physics, Techn. Univ. Delft, Netherlands.

Boundary-Layer Meteorology **60**: 77–93, 1992.

wave pressure pattern was found above the breaking wave, this being the reason for the dramatic increase of form drag.

An additional insight into how breaking waves influence the overlying air flow can be provided on the basis of nonlinear numerical models of turbulent air flow above waves of finite amplitude (Gent and Taylor, 1976; Makin, 1979). The numerical simulation of several laboratory experiments by Makin and Chalikov (1979), Makin (1980b), Makin and Panchenko (1983), Simonov (1982) and McLean (1983) show good quantitative agreement between measurements of velocity and pressure wave fields above waves and the numerical results. In this study, we shall limit ourselves to air flow above monochromatic waves under external forcing conditions being close to Banner's experiment.

The total wind stress at the surface (τ) is formed by the turbulent shear stress (τ^t) and form drag ($\tilde{\tau}^p$), i.e., the correlation between wave-induced pressure perturbation and wave slope. Under laboratory conditions, the turbulent shear stress is produced by small-scale irregularities of the water surface, e.g., wind-driven ripples. It is well known that for the air flow above waves travelling much slower than the wind, the relation $z_0 \cong \frac{1}{30} h_r$ is a good estimate (Kitaigorodskii, 1973). Here, h_r is the characteristic height of the small-scale waves, and z_0 is the local roughness length. This flow corresponds to turbulent flow above immobile roughness elements, and the local drag coefficient (C_1) can be calculated with the usual logarithmic profile:

$$C_1 = \kappa^2 \left[\ln \frac{\Delta z}{z_0} \right]^{-2} .$$

Here, Δz is the distance above the surface. The resulting shear stress can be calculated from a quadratic drag law: $\tau^t \cong C_1 \, \Delta u |\Delta u|$, where Δu denotes wind speed difference over a vertical distance Δz.

The form drag is produced by large-scale wave motions, which are represented in the mentioned experiment by the mechanically generated monochromatic waves. The form drag can be calculated explicitly from surface pressure measurements. Without mechanically generated waves, the air flow in the laboratory is well described by the logarithmic profile:

$$U(z) = \frac{u_*}{\kappa} \ln(z/z_0) ,$$

where the friction velocity u_* is by definition equivalent to $\tau^{1/2} = (\tau^t)^{1/2}$, as $\tilde{\tau}^p = 0$. The air flow above the mechanically generated waves will produce an additional momentum flux, the form drag, resulting in an increased friction velocity, as $\tau^{1/2} = (\tau^t + \tilde{\tau}^p)^{1/2}$. Keeping the mean wind speed far above the wave surface constant and assuming that the profile will stay logarithmic, this results in an increased roughness parameter z_0. This roughness parameter is usually referred to as aerodynamical roughness, as it results from both turbulent friction (described by the local roughness length) and form drag.

We further assume that monochromatic nonbreaking waves do not affect the local roughness. This means that the local roughness length is constant along the wave profile of the monochromatic wave as in the case in which these large-scale waves are absent. For breaking waves, however, we assume that the distribution of small scale irregularities is affected, i.e., the local roughness varies along the profile of the large-scale wave. This assumption is based on the visual impression one gets from a spilling breaker (Kawai, 1982; Bonmarin, 1989, Figure 2; Banner, 1990, Figure 2). The region just beyond the crest is covered with foam, the micro-scale form of the wave profile being highly irregular. Associating these micro-scale irregularities with "roughness elements", we can conclude that the spilling breaker region must have a drastically enhanced local surface roughness.

As the spilling breaker rides at the top of the monochromatic wave, whose phase speed is still a fraction of the wind speed (characteristic values of U/c considered here are between 4 and 8, typical for Banner's experiment), the local roughness in the spilling breaker region can still be estimated by 1/30 of the characteristic height of the local irregularities. This will be specified in Section 3.2. The breaking event (spilling breaker) which occurs at the downwind slope of the wave in the region just beyond the crest will thus be parameterized in the model by increasing the local roughness in this region. In fact, we allow the turbulent stress to increase in the spilling region of the breaker.

First we studied the effect of wave steepness, as it is well known that breaking waves have sharpened crests. Even with a uniform local roughness distribution along the wave profile, we found an important increase of the wave-induced stress (form drag).

Secondly, we pursued the parameterization of the spilling breaker described above. Our results indicate that this mechanism augments the total stress, and it strongly affects the ratio of the wave-induced fluxes to the total flux (which is defined as the coupling parameter α), and the wave growth rate.

The numerical results obtained indicate the increase of total wind stress above steep breaking waves to be of the order of 100%, which is due to the highly asymmetrical pressure pattern which is formed above steep waves and especially above breaking waves. Our results confirm the conclusion of Banner (1990) that the increase of total wind stress above steep breaking waves is due to the increase of form drag, and they are in good quantitative agreement with his measurements. We conclude also that the increase of form drag is due to a highly asymmetrical pressure pattern above the breaking wave, the formation of which can be explained from the increase of steepness of the breaking wave and of the local roughness in the spilling region.

2. Description of the Two-Dimensional Numerical Model

The approach is to consider a two-dimensional air flow over periodic progressive waves. Turbulence is parameterized in terms of eddy viscosity models. We calculate a stationary solution in a frame of reference moving with the wave form,

including the influence of surface roughness and wave form. During the time integration, we pass a transient state starting from an assumed logarithmic velocity profile. The model is based on the full nonlinear Reynolds equations for the air flow, derived in the curvilinear coordinate system $(x, \xi = (z - \eta)/(h - \eta))$. Here, x denotes the horizontal coordinate, z is the height above the mean water level, $\eta(x, t)$ the water surface elevation. t denotes time and h is the height of the atmospheric boundary layer. We shall use the notation $H \equiv h - \eta$. Details of averaging the Navier–Stokes equations can be found in Chalikov (1978). We prefer to use the equations in nondimensional form. The velocity scale is U, denoting the mean wind speed at the upper boundary ($z = h$; $\xi = 1$), where the influence of the waves has been smoothed ($h \gg \eta_{\max}$). We further use the acceleration of gravity g and the air density ρ to construct the other scales. For length, we use U^2/g, for time U/g, for pressure and turbulent stresses ρU^2. The Reynolds equations become:

$$\frac{\partial u}{\partial t} + \frac{1}{H}\frac{\partial H}{\partial t}u + F_u^a + F_u^t = -\frac{\partial P}{\partial x} + \frac{\partial \eta}{\partial x}(1 - \xi)\frac{\partial P}{\partial \xi}, \tag{1}$$

$$\frac{\partial w}{\partial t} + \frac{1}{H}\frac{\partial H}{\partial t}w + F_w^a + F_w^t = -\frac{\partial P}{\partial \xi}. \tag{2}$$

In (1) and (2), F_u^a and F_w^a are the advection terms:

$$F_u^a = \frac{1}{H}\frac{\partial uuH}{\partial x} + \frac{1}{H}\frac{\partial uW}{\partial \xi}, \tag{3}$$

$$F_w^a = \frac{1}{H}\frac{\partial uwH}{\partial x} + \frac{1}{H}\frac{\partial wW}{\partial \xi}, \tag{4}$$

in which:

$$W \equiv w - (1 - \xi)\left(\frac{\partial \eta}{\partial x}u + \frac{\partial \eta}{\partial t}\right). \tag{5}$$

The turbulent terms F_u^t and F_w^t represent:

$$F_u^t = \frac{\partial \overline{u'u'}}{\partial x} + \frac{1}{H}\frac{\partial \overline{u'w'}}{\partial \xi} - \frac{1}{H}\frac{\partial \eta}{\partial x}(1 - \xi)\frac{\partial \overline{u'u'}}{\partial \xi}, \tag{6}$$

$$F_w^t = \frac{\partial \overline{u'w'}}{\partial x} + \frac{1}{H}\frac{\partial \overline{w'w'}}{\partial \xi} - \frac{1}{H}\frac{\partial \eta}{\partial x}(1 - \xi)\frac{\partial \overline{u'w'}}{\partial \xi}. \tag{7}$$

The variable P denotes the deviation from the hydrostatic pressure, and $\overline{u'u'}$, $\overline{u'w'}$, $\overline{w'w'}$ are the turbulent stresses. The continuity equation takes the form:

$$\frac{\partial uH}{\partial x} + \frac{\partial}{\partial \xi}\left[w - u(1 - \xi)\frac{\partial \eta}{\partial x}\right] = 0. \tag{8}$$

2.1. Parameterization of turbulence

The single-point second-order moments in (6) and (7) are usually expressed in terms of the deformation tensor components of the velocity field Φ_{ij} and the isotropic coefficient of turbulent viscosity K:

$$\overline{u_i' u_j'} = \tfrac{2}{3} e \delta_{ij} - K \Phi_{ij} . \tag{9}$$

Here, e represents the total turbulent kinetic energy per unit mass, δ_{ij} is the Kronecker delta and (u_1, u_2) corresponds to the vector (u, w).

$$\begin{aligned} \Phi_{11} &= \frac{2}{H}\left[\frac{\partial uH}{\partial x} - \frac{\partial \eta}{\partial x}\frac{\partial}{\partial \xi}(u(1-\xi)\right], \\ \Phi_{12} = \Phi_{21} &= \frac{1}{H}\left[\frac{\partial u}{\partial \xi} + \frac{\partial wH}{\partial x} - \frac{\partial \eta}{\partial x}\frac{\partial}{\partial \xi}(w(1-\xi))\right], \\ \Phi_{22} &= \frac{2}{H}\frac{\partial w}{\partial \xi} . \end{aligned} \tag{10}$$

We assume that the production of turbulent energy in the boundary layer is balanced by its dissipation to heat:

$$\text{Prod} = K(\tfrac{1}{2}\Phi_{ij}\Phi_{ij}) \tag{11}$$

$$\text{Dissipation } \epsilon = K^3 l^{-4} \tag{12}$$

where $l = \kappa \xi h$ is the length scale for turbulence, and $\kappa = 0.4$ the von Karman constant. From this assumption, we immediately find an expression for K:

$$K = l^2(\tfrac{1}{2}\Phi_{ij}\Phi_{ij})^{1/2} . \tag{13}$$

Note that over a flat surface in a logarithmic boundary layer, (13) simply transforms to $K = l^2|\partial u/\partial z|$. Thanks to this expression for K (13), we do not need to solve the equation for the evolution of turbulent kinetic energy (Chalikov, 1986) because the pressure in (1) and (2) can be redefined as $p = P + \frac{2}{3}e$.

To calculate the turbulent fluxes at the surface $\xi = 0$, we use the square friction law, which can be derived in the curvilinear coordinate system assuming the local turbulent fluxes of momentum and τ_u and τ_w to be constant in a thin sublayer $0 \leq \xi \leq \xi^+$, where ξ^+ is of the order of the height of the molecular viscous sublayer.

$$\begin{aligned} \tau_u &= -\overline{u'w'} + \frac{\partial \eta}{\partial x}\overline{u'u'} - \frac{2}{3}e\frac{\partial \eta}{\partial x}, \\ \tau_w &= -\overline{w'w'} + \frac{\partial \eta}{\partial x}\overline{u'w'} - \frac{2}{3}e . \end{aligned} \tag{14}$$

The turbulent viscosity in this region can be expressed as:

$$K = C_l^{1/2} \cdot l \,, \tag{15}$$

where

$$C_l = \kappa^2 \left[\ln \frac{\xi^+ h}{z_0} \right]^{-2} , \tag{16}$$

is a local drag coefficient and z_0 the local roughness parameter, which is allowed to vary along the x-axis. Integrating (14) over ξ and using (15) and (16), we find:

$$\begin{aligned} \tau_u &= C_l |\Delta u| \left(\Delta u - \frac{\partial \eta}{\partial x} \Delta w + 2 \left(\frac{\partial \eta}{\partial x} \right)^2 \Delta u \right) , \\ \tau_w &= C_l |\Delta u| \left(2\Delta w - \frac{\partial \eta}{\partial x} \Delta u + \left(\frac{\partial \eta}{\partial x} \right)^2 \Delta w \right) . \end{aligned} \tag{17}$$

Here the operator Δ denotes the difference between the value at the level $\xi = \xi^+$ and the value at $\xi = 0$.

2.2. Wave surface, boundary and initial conditions

It is possible to represent a wave surface as a sum of many modes to simulate the sea waves (Makin, 1987). Here, we are interested in the flow pattern above an individual (disturbed) wave. We prescribe the wave surface as a monochromatic Stokes wave to order (a^2), travelling with a constant phase speed c.

$$\eta(x') = a \cdot \cos(kx') + \tfrac{1}{2} a^2 k \cdot \cos(2kx') \,, \tag{18}$$

where $x' = x - ct$.

In (18), a denotes the wave amplitude, $k = 2\pi/\lambda$ is the wave number and λ is the wave length, related to frequency ω by the dispersion relation for deep water gravity waves. In terms of our nondimensional variables, this relation is:

$$\omega^2 = k \,. \tag{19}$$

To solve the set of Equations (1),(2),(8), we need the following boundary conditions. At the wave surface:

$$\xi = 0 \,(z = \eta): \qquad u = u_0, \quad w = w_0 \,. \tag{20}$$

At the upper boundary:

$$\xi = 1 \,(z = h): \qquad u = 1, \quad w = 0 \,. \tag{21}$$

We assume periodicity over the horizontal domain, so we shall use cyclic boundary conditions for x. The components of wave orbital velocity at the surface (u_0, w_0) corresponding to the wave surface (18) are:

$$u_0(x') = a\omega \cdot \cos(kx')$$

$$w_0(x') = a\omega \cdot \sin(kx')[1 + ak \cdot \cos(kx')] \,. \tag{22}$$

In order to reduce the number of external parameters, we set the height of the boundary layer equal to the length of the water wave ($h = \lambda$), so the velocity scale is $U_\lambda \equiv U(z = h)$. One may set the upper boundary height equal to λ, because the wave-induced stress has vanished there. Model tests with upper boundary height set to $0.5 \cdot \lambda$ and to $2 \cdot \lambda$ showed very small differences. Banner (1990) mentioned that in his experiments, the presence of an open or a closed roof section appeared to have only a minor influence on the wave-induced pressure field. Also in his Figure 9b, the wave-induced pressure is practically zero at $z = 13$ cm, while the corresponding wavelength is 21 cm.

The solution depends on three external nondimensional parameters: C_τ – the initial drag coefficient, U_λ/c – the inverse wave-age parameter (equivalent to nondimensional wave frequency ω), and wave slope ak. Note that the drag coefficient is not a fixed parameter. C_τ is only used to specify the roughness length z_0 by assuming a logarithmic profile:

$$C_\tau^{-1/2} = \frac{1}{\kappa} \ln(h/z_0) \,, \tag{23}$$

and to calculate the initial value for the friction velocity:

$$u_* = C_\tau^{1/2} \,. \tag{24}$$

Only z_0, ak and U_λ/c are kept constant during a simulation run. Here, z_0 represents the local roughness which is used in (16), The initial conditions are:

$$t = 0: \qquad u = \frac{u_*}{\kappa} \cdot \ln\left(\frac{\xi h}{z_0}\right); \qquad w = 0 \,. \tag{25}$$

In fact, this initial condition matches the laboratory airflow in the case of an absence of mechanically generated waves. So, z_0 is only connected with the small-scale roughness elements (ripples). More details on the numerical solution can be found in Chalikov (1986) and in Makin (1989). Here, we shall only mention two major characteristics of the method. We use the new coordinate $x' = x - ct$ to search for a stationary solution. We increase the vertical resolution near the surface (the most important region for wind-wave interaction) by transformation of the vertical coordinate ξ:

$$\xi' = \ln\left(\frac{\xi + \chi_0}{\chi_0}\right) . \tag{26}$$

The shrinking parameter χ_0 was set to 0.025. The size of the numerical grid is 16(horizontal) × 21(vertical) points.

2.3. Momentum fluxes

We can introduce the averaging procedure:

$$\langle f(\xi)\rangle = \frac{1}{\lambda}\int_0^{\lambda} f(x,\xi)\,\mathrm{d}x\,, \tag{27}$$

so that:

$$f(x,\xi) = \langle f(\xi)\rangle + \tilde{f}(x,\xi)\,, \tag{28}$$

where f is any field above waves, $\langle f\rangle$ its mean and $\tilde{f}$ denotes wave fluctuations. Applying (27) and (28) to (1) provides the evolution equation for the mean horizontal momentum flux.

$$\frac{\partial\langle uH\rangle}{\partial t} = \frac{\partial}{\partial\xi}(\tau^t + \tilde{\tau}^t + \tilde{\tau}^a + \tilde{\tau}^p)\,. \tag{29}$$

The vertical mean fluxes in the right-hand side of (29) are due to mean turbulent stress:

$$\tau^t = -\langle\overline{u'w'}\rangle\,, \tag{30}$$

mean wave turbulent stress:

$$\tilde{\tau}^t = \left\langle\frac{\partial\eta}{\partial x}(1-\xi)\overline{u'u'}\right\rangle, \tag{31}$$

mean wave advection:

$$\tilde{\tau}^a = -\langle\tilde{u}\tilde{W}\rangle\,, \tag{32}$$

and mean correlation of wave pressure field and wave slope:

$$\tilde{\tau}^p = \left\langle\frac{\partial\eta}{\partial x}(1-\xi)\tilde{p}\right\rangle. \tag{33}$$

We define the total wave flux as:

$$\tilde{\tau} = \tilde{\tau}^t + \tilde{\tau}^a + \tilde{\tau}^p\,. \tag{34}$$

In the steady state, the total momentum flux must be constant over the boundary layer.

$$\tau = \tau^t + \tilde{\tau} = \text{const.} \tag{35}$$

At the upper boundary, the wave flux vanishes: $\tilde{\tau}_1 = 0$. From (35) then follows:

$$\text{const.} = \tau = \tau_1^t = -\langle\overline{u'w'}\rangle_1 = C_D\,. \tag{36}$$

Note that for the initial logarithmic boundary layer, the total flux is:

$$\tau = \tau^t = C_\tau\,, \tag{37}$$

constant over the boundary layer. Due to the development of wave fluxes, C_τ is not equal to the final drag coefficient C_D.

It should be noted that we do not solve the equations for water motion, and therefore we don't have a direct dynamic coupling between wind and waves. The feedback from the waves, however, is expressed in the reconstruction of the vertical structure of the total momentum flux, due to the formation of mean wave-induced fluxes (Equations (29)–(33)). The eddy viscosity coefficient is also allowed to be influenced by waves (Equations (10), (13)). Both mechanisms also influence the distribution of the mean velocity profile.

At the surface, $\tilde{\tau}^a = 0$ because $W_0 = 0$ due to the kinematic boundary condition:

$$\frac{\partial \eta}{\partial t} = w_0 - \frac{\partial \eta}{\partial x} u_0 \qquad (W_0 = 0)\,. \tag{38}$$

The wave-induced flux and the total momentum flux at the surface can thus be written as:

$$\tilde{\tau}_0 = \tilde{\tau}_0^t + \tilde{\tau}_0^p\,, \tag{39}$$

$$\tau_0 = \tau_0^t + \tilde{\tau}_0\,. \tag{40}$$

Their ratio can be considered as a coupling parameter:

$$\alpha = \tilde{\tau}_0/\tau_0\,. \tag{41}$$

Makin and Chalikov (1986, 1991) found that for an old wind sea, α is in the range 0.1–0.2. For a young wind sea, α is between 0.5 and 0.8.

The energy flux to the waves, associated with the momentum flux to the waves, is used to calculate the growth rate of the waves. This wave growth rate or Miles parameter β is defined as:

$$\beta = \frac{\rho}{\rho_w} \frac{\left.\overline{\frac{\partial E}{\partial t}}\right|^w}{E\omega}\,. \tag{42}$$

where $\partial E/\partial t|^w$ is the rate of change in wave energy due to wind, which is defined as $-\langle p_0\, \partial\eta/\partial t\rangle$, ρ_w is the water density and ω is the angular wave frequency. E denotes the total wave energy: $E = \langle \eta^2 \rangle$.

3. Application of the Model to Disturbed or Breaking Waves

The model is suitable for investigating air flow over disturbed waves, because several characteristics like wave form and roughness length can be adapted. Experimental evidence from Banner (1990) led us to vary the local roughness length along the wave surface and the steepness of the breaking wave. We shall present

our results in terms of α (coupling parameter), β (growth rate) and C_D/C_τ (ratio of final and initial drag coefficient).

3.1. Wavelike roughness distribution

At first, we prescribed a sine-wave distribution of the roughness length z_0 along the wave, with the same wavelength as the water wave and amplitude $0.5z_{0r}$. The roughness length thus ranged from $0.5z_{0r}$ to $1.5z_{0r}$, where z_{0r} is the mean and reference value. This method was used to get an idea about the influence of variation of z_0 and to find out which part of the wave is the most sensitive for enhancement of the surface roughness. The distribution function is given by:

$$z_0(x') = z_{0r}(1 + A\cos(kx' - \varphi)) \qquad A = 0.5\,, \tag{43}$$

where z_{0r} denotes the reference roughness calculated from C_τ. The maximum values for β were found for a two or three gridpoint phase shift ($\varphi = 51$ or 77 deg) between η and z_0 ($ak = 0.1$), depending on U_λ/c. The value $\varphi = 77°$ corresponds to $U_\lambda/c = 2$, $\varphi = 51°$ to $U_\lambda/c = 3$, 5 and 10. We define a reference value β_0 for the undisturbed case ($A = 0$). The ratio $\beta_{\max}/\beta_0$ was found to decrease slightly with increasing U_λ/c: from 1.50 at $U_\lambda/c = 2$ to 1.27 at $U_\lambda/c = 10$ ($C_\tau = 0.003$). Also, $\beta_{\max}/\beta_0$ increased with increasing z_{0r}: from 1.32 at $C_\tau = 0.002$ to 1.50 at $C_\tau = 0.003$ ($U_\lambda/c = 2$).

The most important conclusion from these calculations is that enhancing the wave surface roughness influences the momentum and energy fluxes to the waves considerably, and that the part of the wave surface between the crest and the first downwind zero-crossing is the most sensitive part. It is interesting to notice that this most sensitive wave phase quadrant coincides with the place where whitecaps are usually observed. As a result, we presume that a sudden increase in z_0 in this area must have a large impact on the vertical momentum flux.

3.2. Sudden roughness jump

The second approach is based on the pure visual impression one gets from a spilling breaker. The region just beyond the crest is characterized by small-scale irregularities and must have a drastically enhanced local surface roughness. Quantifying this increase is not easy, but using the laboratory results from Banner (1986), we can have an estimate of the increase of the roughness in the spilling region of the breaker.

The local roughness length z_0 can be connected with the characteristic height of the surface irregularities h_r: $z_0 \cong h_r/30$ (see e.g., Kitaigorodskii, 1973). Assuming that $h_r \cong h_b$, which is the characteristic spilling breaker height (reported by Banner (1986) to be 1/50 of the wave length), we found an estimate for the local roughness of the spilling region: $z_0 = 0(10^{-4}\,\text{m})$. For cases with wind ripples only, z_0 is found to be $0(10^{-5}\,\text{m})$. The increase of the local roughness in the spilling region should thus be about one order of magnitude.

As a result, we decided to set the local roughness length to ten times its initial

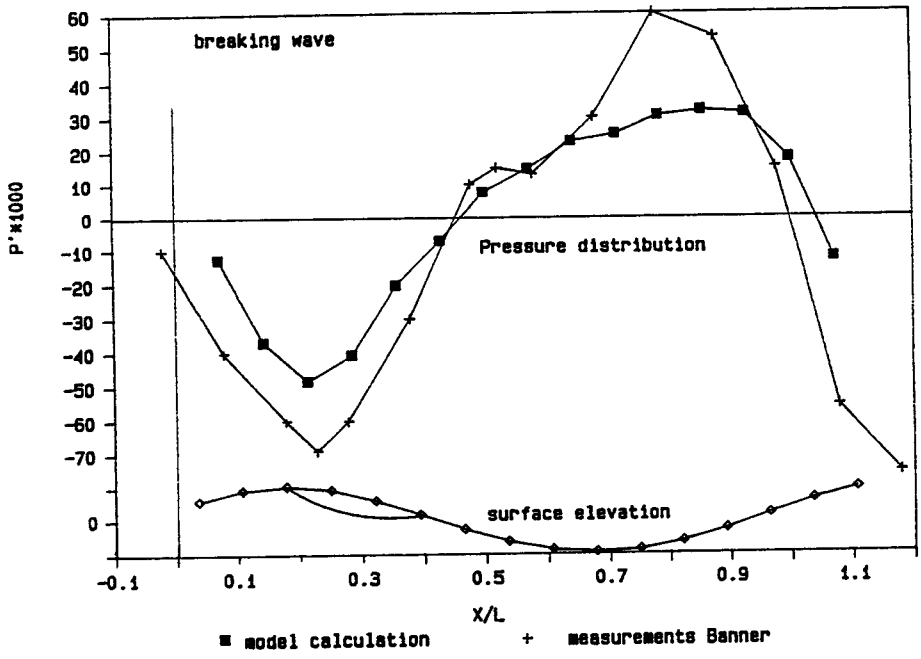

Fig. 1. Surface pressure distribution for a breaking wave. Comparison between laboratory measurements and numerical model calculations. Surface elevation with spilling area.

value at three gridpoints, corresponding to 77 deg of the wave phase, starting at the wave crest, extending downstream. We think that increasing z_0 in the spilling region by one order of magnitude is realistic. It also turned out that the model is not very sensitive for the factor of z_0 increase. We did a few runs with z_0 set equal to five times the reference value and found that the effect was not significantly weaker.

An important result of this locally stepwise enhanced surface roughness is that we found a very pronounced asymmetry in the pressure distribution just above the surface of a wave with a spilling region. Banner (1990) measured the pressure close to the surface of a spilling breaker in a laboratory wave tank. The pressure distribution he measured shows the same characteristic pattern we found from the numerical model calculations. In Figure 1 we compare the results from Banner (1990) (his Figure 10) with our calculations for $ak = 0.3$, $U_\lambda/c = 5$ and $C_\tau = 0.002$. These values approximate the laboratory stationary breaking wave conditions, although the circumstances are not fully compatible. Differences to be mentioned are: asymmetric wave profile in the wave tank, and only one spilling breaker, while in the model we have in fact an infinite row of breaking waves, due to the horizontal cyclic boundary condition. Nevertheless, the basic boundary conditions are similar. As a result, we were encouraged when we found that the calculated pressure distribution compared rather well with the experimental one. It is clear that this pressure distribution considerably enhances the form drag τ^p, which

TABLE I

Numerical model results. The suffix 3 refers to breaking wave, r refers to reference run (see text), and 0 refers to the undisturbed case

C_τ	U_λ/c	$10^4\beta_3$	$10^4\beta_r$	$10^4\beta_0$	C_{D3}/C_τ	C_{Dr}/C_τ	C_{D0}/C_τ	α_3	α_r	α_0
$ak = 0.1$										
	2	3.55	1.8	1.8	1.39	1.21	1.06	0.09	0.06	0.06
$3 \cdot 10^{-3}$	5	38.8	18.3	17.6	1.42	1.24	1.09	0.15	0.09	0.09
	5*	36.5	18.0	17.6	1.38	1.19	1.09	0.14	0.09	0.09
	10	175	87.4	82.9	1.46	1.26	1.10	0.16	0.10	0.11
	2	3.13	1.55	1.5	1.40	1.19	1.08	0.12	0.07	0.08
$2 \cdot 10^{-3}$	5	28.2	14.7	14	1.46	1.23	1.11	0.16	0.10	0.11
	10	123	68.5	65	1.51	1.25	1.13	0.17	0.12	0.12
$1 \cdot 10^{-3}$	2	1.48	1.04	0.99	1.28	1.18	1.11	0.12	0.09	0.10
	10	54.7	45.2	44	1.37	1.28	1.20	0.16	0.15	0.15
$ak = 0.3$										
$3 \cdot 10^{-3}$	5	24.5	17.8	16.8	2.08	1.79	1.63	0.58	0.51	0.53
	10	114	86.4	80.2	2.30	1.97	1.79	0.61	0.56	0.57
$2 \cdot 10^{-3}$	5	19.8	14.4	13.9	2.41	1.99	1.89	0.61	0.55	0.56

*: z_0 in the spilling area set to 5 times the undisturbed value.

implies that the total stress must also increase. We investigated how this phenomenon shows up in the values of the total stress, the wave growth rate β and the coupling parameter α.

It should be noted that the value for z_0 is calculated from the initial condition C_τ. Afterwards, the roughness is locally enhanced. The mean local roughness (not to be confused with aerodynamic roughness, which is associated with the total stress, including form drag) thus also increases, which will also enhance the total stress. In order to separate this effect from the asymmetry effect (which causes enhanced form drag), we also carried out reference runs with a uniform but enhanced roughness distribution. The new value for the initial drag coefficient, $C_{\tau,e}$ was made to fit the same local roughness length as in the simulation of a spilling breaker. In order to achieve the same value for the turbulent stress τ^t as in the breaking wave case, we should use the same value for $\langle \ln(z_0) \rangle$, where $\langle . . \rangle$ denotes the average, as defined in Equation (27). This provides, for example, $C_{\tau,e} = 3.45 \cdot 10^{-3}$, if $C_\tau = 3 \cdot 10^{-3}$ and z_0 is set equal to 10 times its standard value at 3 gridpoints.

In Table I the calculated values for α, β and total stress are shown, also for the reference runs with uniform roughness. The suffix 0 refers to the undisturbed case, the suffix r to the reference run with enhanced uniform roughness and the suffix 3 refers to the breaking wave simulation with z_0 set equal to 10 times the undisturbed value at 3 gridpoints. In Figures 2 and 3, the distribution of surface pressure is shown for undisturbed, reference and breaking cases for the moderate slope wave with $ak = 0.1$ and for the steep wave with $ak = 0.3$.

From Table I and Figure 2 it is clear that the wave-induced stress increases

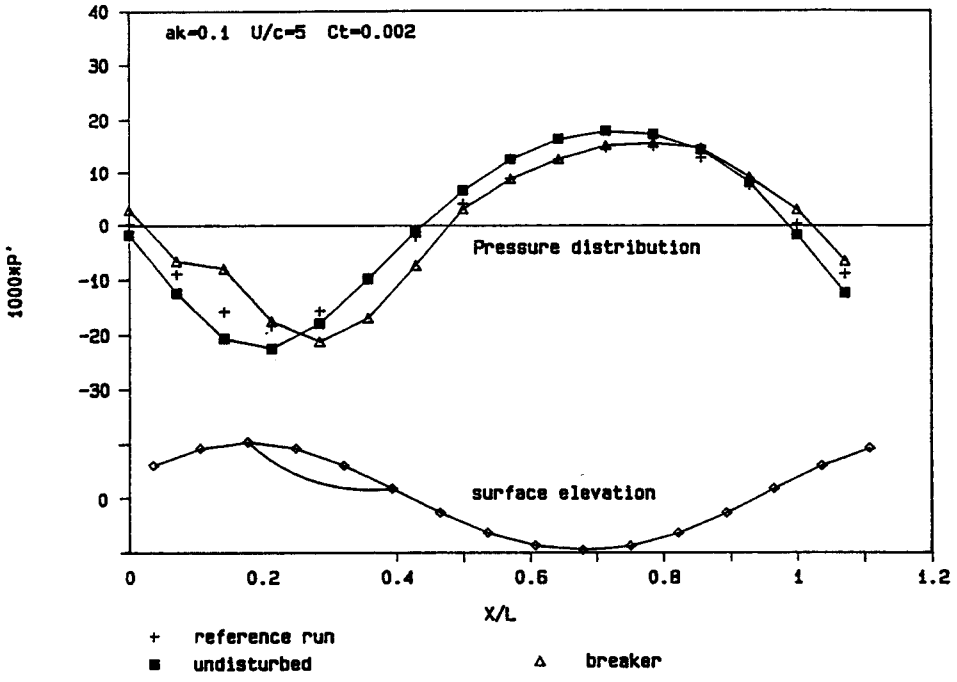

Fig. 2. Surface pressure distribution for a moderately steep wave. Comparison between undisturbed wave, reference run (uniformly enhanced roughness) and spilling breaker.

significantly over a breaking wave with moderate slope $ak = 0.1$. The coupling parameter α was found to decrease slightly when the roughness was uniformly enhanced (α_r In Table I). This can be explained from the increase of turbulent stress due to the enhanced roughness, while there is still no mechanism to increase the wave-induced stress proportionally. The α_3 values as well as the β_3 values, however, are significantly higher than the uniform roughness cases. Obviously, the strong asymmetry effect of the breaking region has a large impact on the wave-induced stress.

The total drag coefficient is also clearly enhanced up to a 35% increase over breaking waves, but this is partly caused by the uniformly enhanced roughness (reference run). If we consider the total stress only, the asymmetry effect is not very important, but looking in more detail, we can conclude that for the wave growth rate, a phase shift between the pressure and the wave pattern is extremely important. From comparison with the undisturbed wave (Table I), it follows that the increase of momentum transfer is partly due to the augmentation of the mean local roughness. However, only the asymmetrical pressure pattern associated with enhanced roughness in the spilling region of a breaking wave is responsible for the drastic increase of the β parameter. In the case of a uniformly enhanced roughness (reference run) the wave momentum flux is small (small α) and the enhanced momentum flux must disappear into currents.

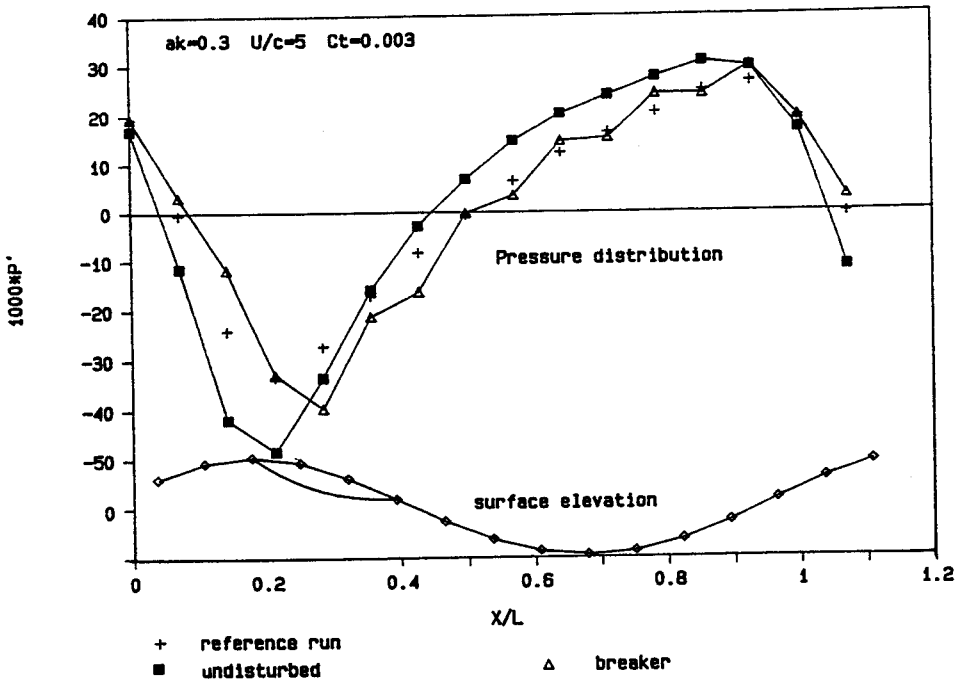

Fig. 3. Surface pressure distribution for a steep wave. Comparison between undisturbed wave, reference run (uniformly enhanced roughness) and spilling breaker.

TABLE II

Phase shift between pressure extremum and crest/trough (deg)

$U_\lambda/c = 5$		φ_0	φ_r	φ_3
$ak = 0.1$	max-trough	13	13	39
$C_\tau = 2 \cdot 10^{-3}$	min-crest	13	13	39
$ak = 0.3$	max-trough	64	90	90
$C_\tau = 3 \cdot 10^{-3}$	min-crest	13	13	39

We found the phase shift of the pressure maximum relative to the trough to be about 39° (see Table II). For the undisturbed case as well as for the reference run, the phase shift is only 13°. From Table II it is evident that the phase shift of the pressure minimum from the crest above a spilling breaker (13° for a nonbreaking wave and 39° for a breaker) increases the correlation between pressure and wave surface. With decrease of U_λ/c and C_τ, the effect on energy and momentum fluxes becomes less pronounced.

The case with steep waves is different (see Figure 3). Even for the undisturbed case, the sharpening of the wave crest leads to a drastic increase of the total wind stress and an asymmetrical pressure pattern is formed. The spilling breaker contributes about 10% to the increase of α and about 30–40% to the increase of β, compared to the reference case. The phase shift of the pressure maximum for

steep breaking waves is 90°, while Banner (1990) reports for the same slope about 60–75°. So it is clear that for steep breaking waves, the effect of enhanced wave slope on the wave-induced stress is rather important: steep waves cause a considerable form drag. The increased local roughness in the spilling area further increases the stress and β, although the effect is less pronounced than for moderately steep waves. This supports the conclusion of Gent and Taylor (1976) that the effect of varying z_0 decreases with increasing wave slope, although we did not find that the effect on β is negligible for steep waves.

From Table II it can be seen that the increase of form drag because of a spilling breaker is due to the phase shift of pressure minimum from the wave crest, being about 39° for the breaking wave and only 13° for the reference and nonbreaking wave. So the spilling breaker shifts the pressure minimum away from the crest, while the pressure maximum is shifted away from the trough by the increase of wave steepness. It is clear that both phase shifts strongly enhance the correlation between pressure and wave slope and thus enhance the wave momentum flux to the waves. The typical value for α, the ratio of the wave momentum flux to the waves and the total stress, was found to be about 0.6, while Banner (1986) reports 0.4.

4. Conclusions

The breaking event (spilling breaker) usually occurs at the downwind slope of steep waves, just beyond the sharpened crest. We studied the air flow above breaking waves using a nonlinear numerical model. The breaking event was parameterized by enhancing the local roughness and changing the wave slope. We found that both mechanisms influence the form drag and the total wind stress. Our calculations indicate that sharpening of the crest of the breaking wave leads to the formation of a highly asymmetrical pressure pattern, the phase shift of the pressure maximum relative to the trough being 90°, while for nonbreaking waves of moderate slope, it is only 13°. This leads to a drastic increase of form drag and, as a result, of the total wind stress, the increase of the latter being typically 100%. The increase of local roughness in the spilling breaker shifts the pressure minimum from the crest, which further increases the form drag and contributes 30 to 40% to the enhancement of β in the case of steep waves.

If the breaking event takes place at a wave of moderate slope, the total stress increases typically by 30%, which is partly due to the increase of mean roughness. The spilling breaker also forms asymmetrical pressure patterns, shifting the pressure minimum from the crest because of the increase of local roughness. This drastically increases the form drag and typically doubles the β parameter. Note that only the wave part $\tilde{\tau}^p$ contributes to wave growth.

Comparison of our numerical results with the measurements of Banner (1986, 1990) shows good agreement on the form of the pressure pattern above steep breaking waves and on the estimates of the form drag and total wind stress. Our

study confirms the conclusion of Banner (1990) that the drastic increase of total wind stress above steep breaking waves is mainly due to the asymmetrical pressure pattern, acting through the increase of form drag.

Knowing the probability function of breaking waves at sea, which will depend on several parameters, it is possible to parameterize the phenomenon by modifying the β parameter. Introducing this modified β parameterization into the integral models of the boundary layer above the sea (Janssen, 1989; Chalikov and Makin, 1991) will lead to improvement of estimates of the drag coefficient and the energy input to the waves, especially for a young wind sea.

The further improvement of the study of breaking waves in the scope of the model presented above needs a more accurate description of the breaking wave form, description of a wave train containing only one or several breaking waves, and clarifying the velocity boundary condition for breaking waves.

Acknowledgements

The authors express their thanks to Profs. J. A. Battjes, D.V. Chalikov and J. Wieringa for their valuable advice. This study was partially supported by the Working Group on Meteorology and Physical Oceanography (MFO) of the Netherlands Organization for the Advancement of Research (NWO).

References

Banner, M. L.: 1990, 'The Influence of Wave Breaking on the Pressure Distribution in Wind-Wave Interactions', *J. Fluid Mech.* **211**, 463–495.

Banner, M. L.: 1986, 'A Comparison of the Wave-Induced Momentum Flux to Breaking and Nonbreaking Waves', in O. M. Phillips and K. Hasselmann (eds.), *Wave Dynamics and Radio Probing of the Sea Surface*, Plenum Press, New York, pp. 321–333.

Bonmarin, P.: 1989, 'Geometric Properties of Deep-Water Breaking Waves', *J. Fluid Mech.* **209**, 405–433.

Chalikov, D. V.: 1978, 'The Numerical Simulation of Wind-Wave Interaction', *J. Fluid Mech.* **87**, 561–582.

Chalikov, D. V.: 1986, 'Numerical Simulation of the Boundary Layer above Waves', *Boundary-Layer Meteorol.* **34**, 63–98.

Chalikov, D. V. and Makin, V. K.: 1991, 'Models of the Wave Boundary Layer', *Boundary-Layer Meteorol.* **56**, 83–99.

Gent, P. R. and Taylor, P. A.: 1976, 'A Numerical Model of the Air Flow above Water Waves', *J. Fluid Mech.* **77**, 105–128.

Janssen, P. A. E. M.: 1989, 'Wave-Induced Stress and the Drag of Air Flow over Sea Waves', *J. Phys. Oceanor.* **19**, 745–754.

Kawai, S.: 1982, 'Structure of Air Flow Separation over Wind Wave Crests', *Boundary-Layer Meteorol.* **23**, 503–521.

Kitaigorodskii, S. A.: 1973, 'The Physics of Air-Sea Interaction', translated from Russian, Israel Program for Scientific Translations, Jerusalem, 273 pp.

Makin, V. K.: 1979, 'The Wind Field above Waves', *Oceanology* **19**, 206–212. (Engl. transl.: *Oceanology* **19**, 127–130).

Makin, V. K.: 1980a, 'Some Results of a Numerical Modeling of Laboratory Experiments to Investigate the Structure of the Air Flow above Waves', *Izv. Akad. Nauk SSSR Atmos. Ocean. Phys.* **16**, 989–991. (Engl. transl.: *Izv. Atm. Oc. Phys.* **16**, 732–734).

Makin, V. K.: 1980b, 'On Energy Transfer to Waves', *Izv. Akad. Nauk SSSR Atmos. Ocean. Phys.* **16**, 549–552. (Engl. transl.: *Izv. Atm. Oc. Phys.* **16**, 382–384).

Makin, V. K.: 1987, 'Wavelike Momentum Fluxes in Boundary Layer above Sea Waves', *Oceanologia* **27**(2). (Engl. transl.: *Oceanology* **27**, 128–132).

Makin, V. K.: 1989, 'The Dynamics and Structure of the Boundary Layer above Sea'. *Senior Doctorate Thesis. Inst. of Oceanology, Academy of Sciences of the USSR. Moscow*, 417 pp. (in Russian).

Makin, V. K. and Chalikov, D. V.: 1979, 'Numerical Modeling of Air Flow Structure above Waves', *Izv. Akad. Nauk SSSR Atmos. Ocean. Phys.* **15**, 292–299. (Engl. transl.: *Izv. Atm. Oc. Phys.* **15**, 199–204).

Makin, V. K. and Chalikov, D. V.: 1986, 'Calculating Momentum and Energy Fluxes Going into Developing Waves', *Izv. Akad. Nauk SSSR Atmos. Ocean. Phys.* **22**, 1309–1316. (Engl. transl.: *Izv. Atm. Oc. Phys.* **22**, 1015–1019).

Makin, V. K. and Panchenko, E. G.: 1983, 'Distribution of Surface Pressure over a surface disturbed by waves'. *Izv. Akad. Nauk SSSR Atmos. Ocean. Phys.* **19**, 1098–1101. (Engl. transl.: *Izv. Atm. Oc. Phys.* **19**, 831–833).

McLean, J. W.: 1983, 'Computation of Turbulent Flow over a Moving Wavy Boundary', *Phys. Fluids* **26**, 2065–2073.

Simonov, V. V.: 1982, 'Calculation of the Form Drag of the Wavy Surface', *Izv. Akad. Nauk SSSR Atmos. Ocean. Phys.* **18**, 269–275. (Engl. transl.: *Izv. Atm. Oc. Phys.* **18**, 206–210).